Phosphorus-bearing molecules in solar-type star-forming regions: first PO detection

Bertrand Lefloch,[1,2,3]★ C. Vastel,[4,5] S. Viti,[6] I. Jimenez-Serra,[6,7] C. Codella,[8] L. Podio,[8] C. Ceccarelli,[1,2] E. Mendoza,[3,1] J. R. D. Lepine[3] and R. Bachiller[9]

[1]*Univ. Grenoble Alpes, IPAG, F-38000 Grenoble, France*
[2]*CNRS, IPAG, F-38000 Grenoble, France*
[3]*IAG, Universidade de São Paulo, Cidade Universitária, SP 05508-090, Brazil*
[4]*Université de Toulouse, UPS-OMP, IRAP, F-31028, Toulouse Cedex 4, France*
[5]*CNRS, IRAP, 9 Av. colonel Roche, BP 44346, F-31028, Toulouse Cedex 4, France*
[6]*Department of Physics and Astronomy, University College London, Gower Street, London WC1E 6BT, UK*
[7]*School of Physics and Astronomy, Queen Mary, University of London, Mile End Road, London E1 4NS, UK*
[8]*INAF, Osservatorio Astrofisico di Arcetri, Largo Enrico Fermi 5, I-50125 Firenze, Italy*
[9]*Observatorio Astronómico Nacional (OAN), Apdo 112, E-28803 Alcalá de Henares, Madrid, Spain*

ABSTRACT

As part of the Large Program Astrochemical Surveys At IRAM, we have used the IRAM 30 m telescope to lead a systematic search for the emission of rotational transitions of P-bearing species between 80 and 350 GHz towards L1157-B1, a shock position in the solar-type star-forming region L1157. We report the detection of several transitions of PN and, for the first time, of pre-biotic molecule PO. None of these species are detected towards the driving protostar of the outflow L1157-mm. Analysis of the line profiles shows that PN arises from the outflow cavity, where SiO, a strong shock tracer, is produced. Radiative transfer analysis yields an abundance of 2.5×10^{-9} and 0.9×10^{-9} for PO and PN, respectively. These results imply a strong depletion (≈ 100) of phosphorus in the quiescent cloud gas. Shock modelling shows that atomic N plays a major role in the chemistry of PO and PN. The relative abundance of PO and PN brings constraints both on the duration of the pre-shock phase, which has to be $\sim 10^6$ yr, and on the shock parameters. The maximum temperature in the shock has to be larger than 4000 K, which implies a shock velocity of $40 \, \mathrm{km \, s^{-1}}$.

Key words: astrochemistry – stars: formation – ISM: abundances – ISM: jets and outflows – ISM: molecules.

1 INTRODUCTION

Despite a rather low elemental abundance of $\sim 3 \times 10^{-7}$ (Asplund et al. 2009), phosphorus is one of the main biogenic elements, present in all life forms on Earth. As such, phosphorus-bearing compounds, in particular, their P–O bonds, play a key role in many biochemical and metabolic processes in living systems (see e.g. Macía 2005, for a review). In our Solar system, the presence of phosphorus has been recently reported in comet 67P/Churyumov–Gerasimenko (Altwegg et al. 2016), although the nature of the actual carriers remain to be identified. Phosphorus-bearing compounds appear to be rather ubiquitous in meteorites (Macía 2005).

A theoretical study by Thorne et al. (1984) based on laboratory experiments predicted that phosphorus monoxide PO should be

the most abundant P-bearing molecule in molecular clouds, hence the main reservoir of phosphorus in the gas phase. Phosphorus monoxyde PO was detected for the first time by Tenenbaum, Woolf & Ziurys (2007) towards the evolved star VY Cma. The P-bearing species HCP, PH_3, CP, CCP radicals, PO, and PN have been identified around evolved stars IRC+10216 (see e.g. Agundez, Cernicharo & Guélin 2007, for a review) and IK Tau (De Beck et al. 2013). PO was found as abundant as PN in the envelope of VY CMa, a fact which led the authors to propose that these species are formed from shocks in the circum-stellar envelope; they also concluded that PO and PN are the main reservoir of phosphorus in the gas phase.

PN was first detected towards a few high-mass star-forming regions: Ori(KL) (Ziurys 1987), W51M and SgrB2 (Turner & Bally 1987). A systematic search for PO by Matthews, Feldman & Bernath (1987) yielded only upper limits in the massive star-forming regions Ori(KL), SgrB2 and DR21(OH). Recently, Fontani et al. (2016) observed a sample of 26 massive cores at various evolutionary stages,

from pre-stellar to ultracompact H II regions and report detection of the PN J = 2–1 line in about 30 per cent of their sample. Rivilla et al. (2016) have reported the first detection of PO towards high-mass star-forming regions and found that phosphorus seems strongly depleted from the gas phase. The first evidence of P-bearing species in low-mass star-forming regions was provided by Yamaguchi et al. (2011), who reported the tentative detection of the PN transition J = 2–1 towards the shock positions B1 and B2 in the outflow of the low-mass Class 0 protostar L1157-mm ($d = 250$ pc). This is the first and only P-bearing molecule tentatively detected in a solar-type star-forming region until now.

Given the importance of phosphorus for pre-biotic chemistry and its presence in the early stages of our own Solar system, we have led a systematic search for the presence of phosphorus-bearing molecules in solar-type star-forming regions, in the framework of the Large Program dedicated to Astrochemical Surveys At IRAM (ASAI; Lefloch & Bachiller, in preparation), with the 30 m telescope. In this paper, we present the results of our study towards the outflow shock L1157-B1 and the driving protostar L1157-mm. No emission was detected towards the protostar. Towards L1157-B1, we have detected the emission of various rotational transitions of PN and of PO, for the first time. A search for more complex P-Bearing species (e.g. PH$_3$) yielded only negative results. After presenting the observational results on our systematic search (Section 2), we derive the physical conditions and molecular abundances for both species, and discuss the implication on their formation and shock chemistry.

2 OBSERVATIONS

The observations of L1157-B1 and L1157-mm were acquired with the IRAM-30m telescope at Pico Veleta (Spain), during several runs in 2011 and 2012. The observed position of L1157-B1 and L1157-mm are $\alpha_{J2000} = 20^h39^m10^s2$, $\delta_{J2000} = +68°01′10″$ and $\alpha_{J2000} = 20^h39^m06^s3$, $\delta_{J2000} = +68°02′15″8$, respectively. The survey was carried out using the broad-band EMIR receivers at 3 mm (80–116 GHz), 2 mm (128–173 GHz) and 1.3 mm (200–272 GHz). Fast Fourier transform spectrometers were connected to the EMIR receivers, providing a spectral resolution of 195 kHz. The high-frequency part of the 1.3 mm band (260–272 GHz) was observed with the WILMA autocorrelator, at 2 MHz resolution. The final kinematic resolution of the FTS data was degraded to 1 km s^{-1}. The observations were carried out in Wobbler Switching Mode, with a throw of 3 arcsec, in order to ensure a flat baseline across the spectral bandwith observed (4–8 GHz, depending on the receiver).

The data reduction was performed using the GILDAS/CLASS90 package.[1] The line intensities are expressed in units of antenna temperature corrected for atmospheric attenuation and rearward losses ($T_A^\star$). For the ASAI data, the calibration uncertainties are typically 10, 15, and 20 per cent at 3, 2, and 1.3 mm, respectively. For subsequent analysis, fluxes were expressed in main-beam temperature units (T_{mb}). The telescope and receiver parameters (main-beam efficiency B_{eff}, forward efficiency F_{eff}, half-power beam width HPBW) were taken from the IRAM webpage.[2] We used in the following the CASSIS software[3] for the line identification.

We have summarized the spectroscopic properties and observational parameters of the lines detected in the Table 1. We show in Fig. 1 a montage of the PO and PN lines detected towards L1157-B1.

3 RESULTS

3.1 PN

We used the spectroscopic parameters provided by Cologne Database for Molecular Spectroscopy (CDMS) for the phosphorus nitride molecule (Cazzoli, Cludi & Puzzarini 2006). The four PN rotational transitions J = 2–1, 3–2, 5–4 and 6–5 fall into the ASAI bands (see Table 1). No emission at all was detected towards L1157-mm (see the J = 2–1 spectrum in red in the bottom panel of Fig. 2). On the contrary, all of them were detected towards L1157-B1, with an SNR between 4 and 10. We confirm the previous detection by Yamaguchi et al. (2011) of the J = 2–1 and report the detection of the transitions J = 3–2, 5–4 and 6–5, from levels with upper energy levels E_{up} up to 47 K. The spectra display a linewidth in the range 4.5–6.2 km s^{-1}, similar to the values measured for several other molecular species (see Codella et al. 2010), which testify of the shock origin of the emission.

The J = 2–1 and 3–2 lines are detected with a typical intensity of 30 mK. The SNR in the wings of the J = 2–1 and 3–2 line profiles is high enough to constrain the slope of the intensity distribution as a function of velocity, following the approach of Lefloch et al. (2012) (see also Gómez-Ruiz et al. 2015). The intensity profile is well-described by an exponential law $\propto \exp{(v/v_0)}$ with $v_0 \approx 4.4$ km s^{-1} (see Fig. 2). As discussed by Lefloch et al. (2012) and Gómez-Ruiz et al. (2015), this slope is the specific signature of the outflow cavity associated with L1157-B1 (g_2). A blueshifted wing is detected up to ≈ -20 km s^{-1} in the PN J = 2–1 line profile (see Fig. 2), and we find a very good match with the SiO J = 2–1 line profile obtained at a similar angular resolution of 27 arcsec with the IRAM 30 m telescope. This suggests that the PN and SiO spatial distributions are very similar, and that PN comes from the region where the impact of the shock on the surrounding material is violent, with velocities larger than ≈ 25 km s^{-1}. This provides us with an estimate for the size of the PN-emitting region ≈ 18 arcsec.

3.2 PO

We searched for all PO transitions in the ASAI bands. We used the spectroscopic parameters for phosphorus monoxide provided by the CDMS data base (Kawaguchi, Saito & Hirota 1983 ; Bailleux et al. 2002). A grand total of twelve PO transitions have $A_{ij} \geq 10^{-5}$ s^{-1} between 80 and 272 GHz. All the transitions fulfilling this criterion in the 3 and 1.3 mm bands were detected. This is the first detection of PO in a solar-type star-forming region. Overall, lines are rather weak, with typical intensities of 5–8 mK. In the 2 mm bands, two line doublets have A_{ij} larger than 10^{-5} s^{-1}. Unfortunately, the higher rms noise in that part of the spectrum (5 mK per interval of 1 km s^{-1}) permits marginal detection of one doublet only. As a result, the flux of the 2 mm transitions is rather uncertain, and we did not take them into account into the subsequent analysis to determine the excitation conditions of the PO gas. The large number of transitions detected (10) makes us confident in the identification of PO in the line spectrum of L1157-B1. The PO line emission peak is located close to ≈ -2 km s^{-1}, i.e. it is shifted from PN by ~ 2–3 km s^{-1} (see Fig. 2). The velocity difference between the PO and PN emission peaks implies that both species probably form in different regions of the shock. We note that the full width at zero

Table 1. Spectroscopic and observational parameters of the molecular transitions of PO and PN observed towards L1157-B1, whose Einstein coefficient of spontaneous emission A_{ij} is larger than 10^{-5} s^{-1}. Uncertainties on the line parameters are given in brackets. Line intensity uncertainties are measured in a velocity interval of 1 km s^{-1}). Upper limits are estimated for a 3σ rms.

	Transition			Frequency (MHz)	E_{up} (K)	HPBW (arcsec)	F_{eff}	B_{eff}	$\int T_A^* dv$ (mK km s^{-1})	V (km s^{-1})	ΔV (km s^{-1})	T_A^* (mK)
PN												
2–1				93 979.7689	6.8	26.2	0.95	0.80	148(13)	−0.24(0.25)	5.97(.70)	23.3(3.0)
3–2				140 967.6921	13.5	17.5	0.93	0.74	186(13)	−0.67(0.23)	6.27(.54)	27.8(3.4)
5–4				234 935.2619	33.8	10.5	0.91	0.58	43(9)	−0.62(.48)	4.31(.88)	9.4(1.5)
6–5				281 914.2033	47.4	8.7	0.88	0.49	28(9)	−1.47(.97)	4.61(2.05)	5.6(2.5)
PO $^2\Pi_{1/2}$												
J – (J – 1)	Parity	F – (F – 1)										
5/2 – 3/2	e	3–2		108 998.445	8.4	22.6	0.95	0.79	63.2(7.0)	−2.18(.37)	7.38(.94)	8.0(1.1)
5/2–3/2	e	2–1		109 045.040	8.4	22.6	0.95	0.79	38.5(7.0)	−3.19(.73)	7.80(1.60)	4.6(1.2)
5/2–3/2	f	3–2		109 206.200	8.4	22.5	0.95	0.79	27.3(6.0)	−2.34(.37)	5.63(.84)	7.9(1.3)
5/2–3/2	f	2–1		109 281.189	8.4	22.5	0.95	0.79	24.5(7.0)	0.20(.63)	5.18(1.90)	4.5(1.1)
7/2–5/2	f	4–3		152 656.979	15.7	16.1	0.93	0.72	118.0(19)	−1.34(.26)	5.60(.99)	19.8(5.4)
7/2–5/2	f	3–2		152 680.282	15.7	16.1	0.93	0.72	66.6(17)	−1.95(1.04)	5.60 (.00)	11.2(5.0)
7/2–5/2	e	4–3		152 855.454	15.7	16.1	0.93	0.72	<35	–	–	<15.0
7/2–5/2	e	3–2		152 888.128	15.7	16.1	0.93	0.72	<35	–	–	<15.0
11/2–9/2	f	6–5		239 948.978	36.7	10.3	0.91	0.58	51.1(6.0)	−1.54(.30)	5.06(.65)	10.0(1.9)
11/2–9/2	f	5–4		239 958.096	36.7	10.3	0.91	0.58	47.1(6.5)	−1.45(.35)	4.86(.79)	9.1(1.9)
11/2–9/2	e	6–5		240 141.054	36.7	10.2	0.91	0.58	14.5(5.3)	−3.04(.43)	2.25(.98)	6.2(2.2)
11/2–9/2	e	5–4		240 152.530	36.7	10.2	0.91	0.58	28.5(9.0)	−4.89(.85)	4.42(1.90)	6.1(2.2)
PH$_3$												
1_0–0_0				266 944.662	12.8	9.2	0.89	0.52	<32	–	–	<9.6(*)

* per interval of 2 MHz (2.25 km s^{-1}).

intensity is approximately 10 km s^{-1}: it is narrower for PO than for PN (20 km s^{-1}).

3.3 PH$_3$

We used the spectroscopic parameters for PH$_3$ provided by the CDMS data base (Müller & Wood 2013). All the rotational transitions of PH$_3$ accessible in the ASAI bands are characterized by very low Einstein coefficients A_{ij}, typically less than 10^{-7} s^{-1} and very high upper level energies E_{up} (typically higher than 60 K). The only transition with favourable excitation conditions is the 1_0–0_0 at 266.944 662 GHz, which has an E_{up}= 12.8 K and an A_{ij} of 3.808×10^{-4} s^{-1}. We failed to detect this transition down to an rms of 3.2 mK (T_A^*) in an interval of 2 MHz. Adopting a typical linewidth of 5 km s^{-1}, we obtain a 3σ upper limit of 32 mK km s^{-1} (in T_A^*) for the line flux.

A search for other P-bearing molecules yielded only negative results.

4 DISCUSSION

4.1 Molecular abundances

Plateau de Bure observations by Gueth, Guilloteau & Bachiller (1998) indicate a typical, round size of 18 arcsec for the SiO J = 2–1 line emission, centred close to the nominal position of L1157-B1. Observations with the IRAM Plateau de bure interferometer at 3 arcsec resolution reveal an inhomogeneous structure with the presence of three compact clumps of gas in L1157-B1, named 'B1a-b-c', with a typical size of 4 arcsec (Benedettini et al. 2013). We have considered two cases in the derivation of the physical conditions and abundance of PO and PN: (a) phosphorus emission arises from the whole shock region detected in SiO J = 2–1 (size = 18 arcsec), as suggested in Section 3.2; (b) phosphorus emission arises from one of the compact clumps present in the SiO shock region (size = 4 arcsec). We adopted a linewidth $\Delta V = 6$ km s^{-1}, in good agreement with the value obtained from a Gaussian fit to the PO and PN line profiles of the J = 2–1 and 3–2 transitions. The corresponding fluxes are listed in Table 1.

4.1.1 PN

We derived the physical conditions in the PN gas from an analysis in the large velocity gradient approximation with the radiative transfer code MADEX. We used the PN–He collisional coefficients from Tobola et al. (2007) and scaled by a factor of 1.37 to take into account the difference in mass of H$_2$.

We first consider the case (a) for the origin of PN emission. We find as best-fitting solution a gas temperature $T_{kin} = 60$ K, $n(H_2) = 9 \times 10^4$ cm^{-3}, and a source-averaged column density $N(PN) = 9.0 \times 10^{11}$ cm^{-2}. The fit of the PN transitions is superposed in red on the line spectra in Fig. 1. A minimum χ^2 analysis shows that best-fitting solutions are obtained for $N(PN) = (9.0 \pm 1.0) \times 10^{11}$ cm^{-2}; the kinetic temperature is not well-constrained and solutions in the range 40–80 K are possible. On the contrary, the density is well-constrained in the range $(0.5$–$1.0) \times 10^5$ cm^{-3}. We note that these physical conditions are consistent with the gas kinetic temperature and the density previously determined in the L1157-B1 cavity, from a CO and CS multitransition analysis (Lefloch et al. 2012; Gómez-Ruiz et al. 2015). Lefloch et al. (2012) estimated a CO gas column density of 1.0×10^{17} cm^{-2} for the L1157-B1 outflow cavity. Adopting a standard abundance ratio [CO]/[H$_2$] = 10^{-4}, we derive the abundance of PN relative to H$_2$ [PN] $\simeq 0.9 \times 10^{-9}$. This value is in reasonable agreement with the previous determination of Yamaguchi et al. (2011): $(0.2$–$0.6) \times 10^{-9}$.
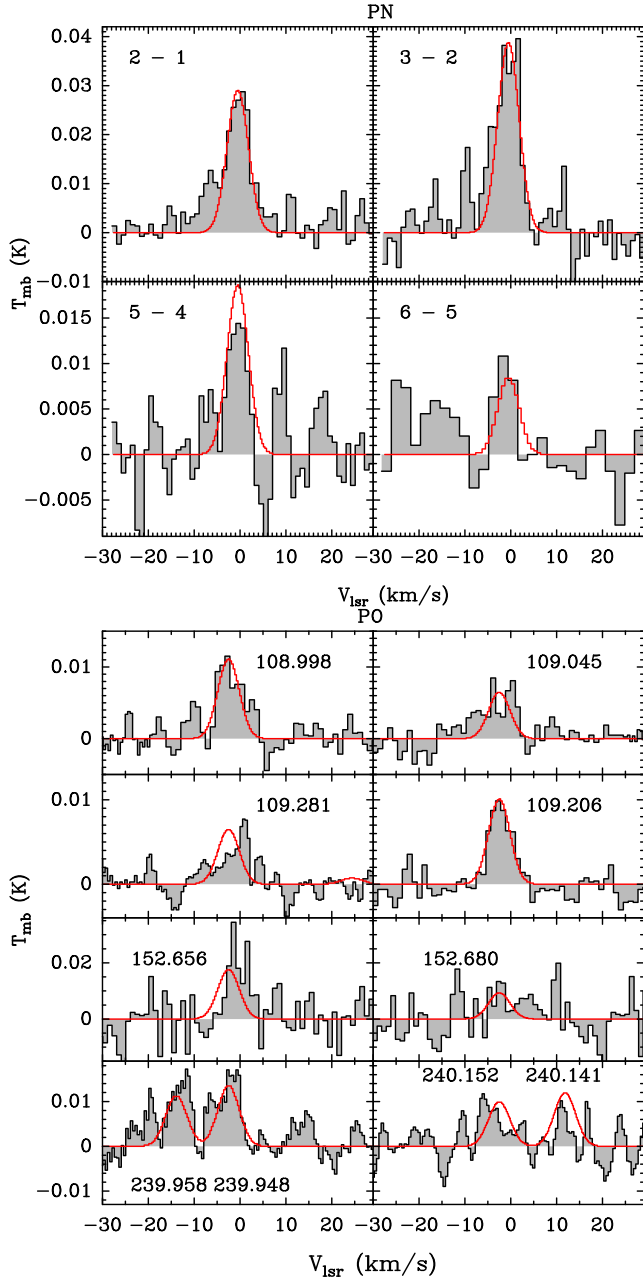
Figure 1. Montage of the PN and PO lines detected towards protostellar shocks L1157-B1. The red curve represents the best fit obtained from the PO and PN line radiative transfer analysis (see Section 4).

Figure 2. From top to bottom: (a) spectral profile of the PN J $= 2$–1 displayed on a lin-log scale. We have superposed in red (blue) a fit to the spectral slope of the type $T_A^*(v) \propto \exp(v/v_0)$ with $v_0 = 4.4\,\mathrm{km\,s^{-1}}$ ($2.2\,\mathrm{km\,s^{-1}}$), corresponding to the signature of components g_2 (g_3) of the outflow. (b) Superposition of the PN J $= 2$–1 (solid) and SiO J $= 2$–1 (dashed red) line profiles. A scaling factor of 0.013 was applied to SiO J $= 2$–1 so to match the PN J $= 2$–1 emission peak. (c) Comparison of the PN J $= 2$–1 (solid) and PO 109.206 GHz (dashed red) lines. (d) Comparison of the PN J $= 2$–1 line emission towards L1157-B1 (solid) and L1157-mm (dashed red). The vertical line in dashed marks the ambient cloud velocity $v_{\mathrm{lsr}} = +2.6\,\mathrm{km\,s^{-1}}$.

4.1.2 PO

Due to the absence of coefficients available for PO–H_2 collisions, we carried out a simple local thermodynamic equilibrium analysis using CASSIS. The column density and the excitation temperature were determined from a best-fitting analysis (χ^2) on the 5/2–3/2 transitions at 3 and 1.3 mm. We could check a posteriori that the lines are optically thin.

Proceeding as above, we first assumed a size of 18 arcsec for the PO-emitting region. The best-fitting solution is obtained for a rotational temperature $T_{\mathrm{rot}} = 12.0 \pm 0.9$ K and a source-averaged column density $N(\mathrm{PO}) = (2.3 \pm 0.4) \times 10^{12}\,\mathrm{cm^{-2}}$, resulting into a gas phase abundance [PO] $\simeq 2.5 \times 10^{-9}$. This is about three times the abundance of PN. The fit to the PO transitions is superposed in red on the line spectra in Fig. 1, with a fixed full width at half-maximum of $5.5\,\mathrm{km\,s^{-1}}$ and v_{lsr} of $-2.5\,\mathrm{km\,s^{-1}}$, with the above parameters.

We now consider the case (b), i.e. the alternative situation where PN arises mainly from one of the shocked gas clumps reported by Benedettini et al. (2013). We then obtain solutions of the type $N(\mathrm{PN}) = 4 \times 10^{13}\,\mathrm{cm^{-2}}$, $n(\mathrm{H_2}) = 1 \times 10^4\,\mathrm{cm^{-3}}$, $T = 55$ K. This would result in a typical abundance [PN] $\simeq 4 \times 10^{-8}$. Such low densities are hard to reconcile with the overall density structure of L1157-B1, as derived by Gómez-Ruiz et al. (2015), or even the density estimates obtained towards the compact clumps reported by Benedettini et al. (2013). Our analysis favours case (a): PN arises from an extended region in the shock, close to the apex of the outflow cavity, where efficient grain sputtering is taking place.
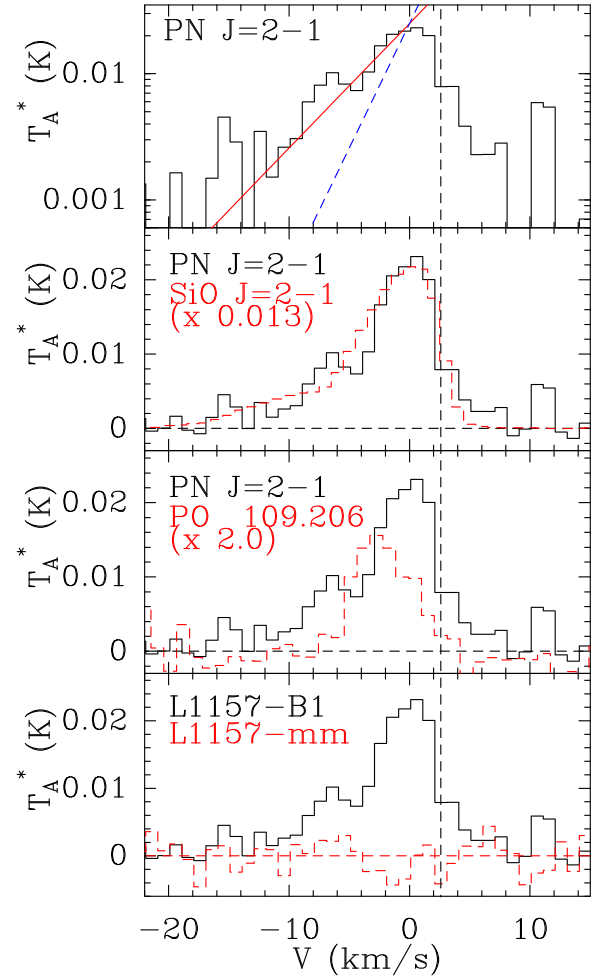
Like for PN, we consider the case where the PO-emitting region would arise from a compact shock region. Not surprisingly, a larger column density is required to account for the PO emission: typically 3×10^{13} and 1.3×10^{14} cm^{-2} for a source size of 4 and 2 arcsec, respectively. This corresponds to a PO abundance [PO] = 3×10^{-8} and 1.3×10^{-7}, respectively.

4.1.3 *PH$_3$*

We used CASSIS to obtain an upper limit on the abundance of phosphine from the non-detection of the ground transition 1_0–0_0 at 266 944.662 GHz. We adopted a typical excitation temperature of 10 K, a linewidth of 5 km s^{-1}, and adopted a typical source size of 18 arcsec. Taking into account the rms of 3 mK, comparison with the ASAI data shows that $N(PH_3)$ has to be less than $\approx 10^{12}$ cm^{-2}, which results into an upper limit of 10^{-9} for the phosphine abundance in the gas phase.

As a conclusion, a careful determination of the abundance of P-bearing species in the gas phase shows that they contain only a few per cent of the total elemental phosphorus.

5 PHOSPHORUS CHEMISTRY IN THE L1157-B1 SHOCK

In Section 3, we showed that the emission from PN and PO arises from the L1157-B1 outflow cavity, which can be described by a C-type shock (Lefloch et al. 2012; Holdship et al. 2016). We therefore investigate the origin of the PO and PN emission in this region by the use of the chemical gas–grain model UCL_CHEM (Viti, Collings & Dever 2004b) coupled with the parametric C-shock model by Jimenez-Serra et al. (2008). We use the same approach as Viti et al. (2011) where we modelled the ammonia and water emission across the same region. We note that a similar approach was used by Aota & Aikawa (2012) to reproduce the previous observations of PN and PO performed by Yamaguchi et al. (2011) towards the same outflow cavity. We stress that our new observational constraints lead to different conclusions about the history of the region and the shock parameters. This point is more specifically addressed in Section 5.3.

We study the evolution of phosphorous-bearing species in a one-dimensional C-shock, but with the specific aim of determining whether PO and PN are mainly formed and destroyed in the gas phase prior to the shock passage, on the grains, or during the shock event(s). Moreover, as in Viti et al. (2011), our model is able to determine whether the differences in line profiles discussed above may be explained by the differences in abundances at different velocities.

5.1 Modelling

A detailed description of UCL_CHEM coupled with the shock model can be found in Viti et al. (2011). Here we briefly summarize the main characteristics of the code. The code is run in two phases, where Phase I forms a dense core out of a diffuse medium, starting from an essentially atomic gas. We adopt an initial density of 100 cm^{-3} for the diffuse medium. During this phase, gas-phase chemistry, freezing on to dust particles and subsequent surface processing, occurs. The sticking efficiency for all species is assumed to be 100 per cent but the rate of depletion is a function of density (in a similar manner as in Rawlings et al. 1992). The density at the end of Phase I is a free parameter, called from now on the pre-shock density. The second phase computes the time-dependent chemical evolution of the gas and dust during the passage of a shock.

The model includes both thermal desorption, due to the dust being heated by the presence of the outflow, as well as sputtering of the icy mantles once the dynamical age across the C-shock has reached the 'saturation time-scales', as in Jimenez-Serra et al. (2008). The saturation time-scale corresponds to the time when most of the ices have been injected into the gas phase, due to the passage of the shock (Jimenez-Serra et al. 2008). Such time-scales are inversely proportional to the density of the gas and for pre-shock H$_2$ densities of 10^4–10^5 cm^{-3}, these times range between 10 and 100 yr, i.e. factors 10–100 shorter than the typical dynamical ages of young molecular outflows (10^3 yr). Our chemical gas-phase network is taken from UMIST 12[4] and is augmented with updates from the KIDA data base.[5] The surface network comprises mainly hydrogenation reactions. In particular, we note that neither UMIST 12 nor KIDA contains a network for PH$_3$. Rather than creating an ad hoc set of reactions for this species, we made the assumptions that this species will be preferentially formed on the grains by hydrogenation and that therefore PH$_2$ could act as a proxy for PH$_3$. Of course, this also means that we are assuming that the routes for gas-phase destruction for PH$_3$ and PH$_2$ are similar. In all our figures, we therefore present PH$_2$ as a proxy for PH$_3$.

We ran a small grid of models where we varied:

(i) the pre-shock density; we have adopted two possible values for the total hydrogen nuclei density n (H+2 × H$_2$) based on previous studies of this cavity: 10^4 and 10^5 cm^{-3}.

(ii) the shock velocity, from 20 to 40 km s^{-1}. From the pre-shock density and the shock velocity, the maximum temperature of the neutral fluid attained within the shock is taken from figs 8(b) and 9(b) in Draine, Roberge & Dalgarno (1983).

(iii) the initial elemental abundance of phosphorous: while its abundance in the diffuse, warm interstellar medium, is found to be solar (e.g. Jenkins, Savage & Spitzer 1986), all the studies so far of phosphorous-bearing species in star-forming regions have found that the initial elemental abundance of phosphorous needs to be depleted by up to a factor of 100 in order to match the observations (Aota & Aikawa 2012; Fontani et al. 2016; Rivilla et al. 2016). We have therefore varied this parameter and adopted values of solar (2.57×10^{-7}) down to a depletion factor of 100.

(iv) the duration of the pre-shock phase (Phase I). We have considered a short-lived and a long-lived scenario, respectively, to investigate the impact of different initial gas compositions, as a result of different cloud ages. In the first case, the core is immediately subjected to the passage of a shock when it reaches the pre-shock density; in the second case, the core is allowed to remain static for about 2 million yr.

5.2 Results

The observations yield abundance values for PO and PN of the order of 1–3×10^{-9}, for a common source size of 18 arcsec, with PO larger by a factor of 3 or so than PN. PH$_3$ is undetected, and has an upper limit of 10^{-9}. We present in Fig. 3 the evolution of phosphorous bearing species as well as nitrogen as a function of time during the passage of the shock (Phase II), when the initial elemental abundance of phosphorus is depleted by a factor of 100 and the pre-shock phase is long-lived. We show the result for three shock velocities (20, 30, 40 km s^{-1}), pre-shock densities of 10^4 and 10^5 cm^{-3}, and long-/short-lived pre-shock phase in Figs 3 and 4,

---

[4] http://udfa.ajmarkwick.net/
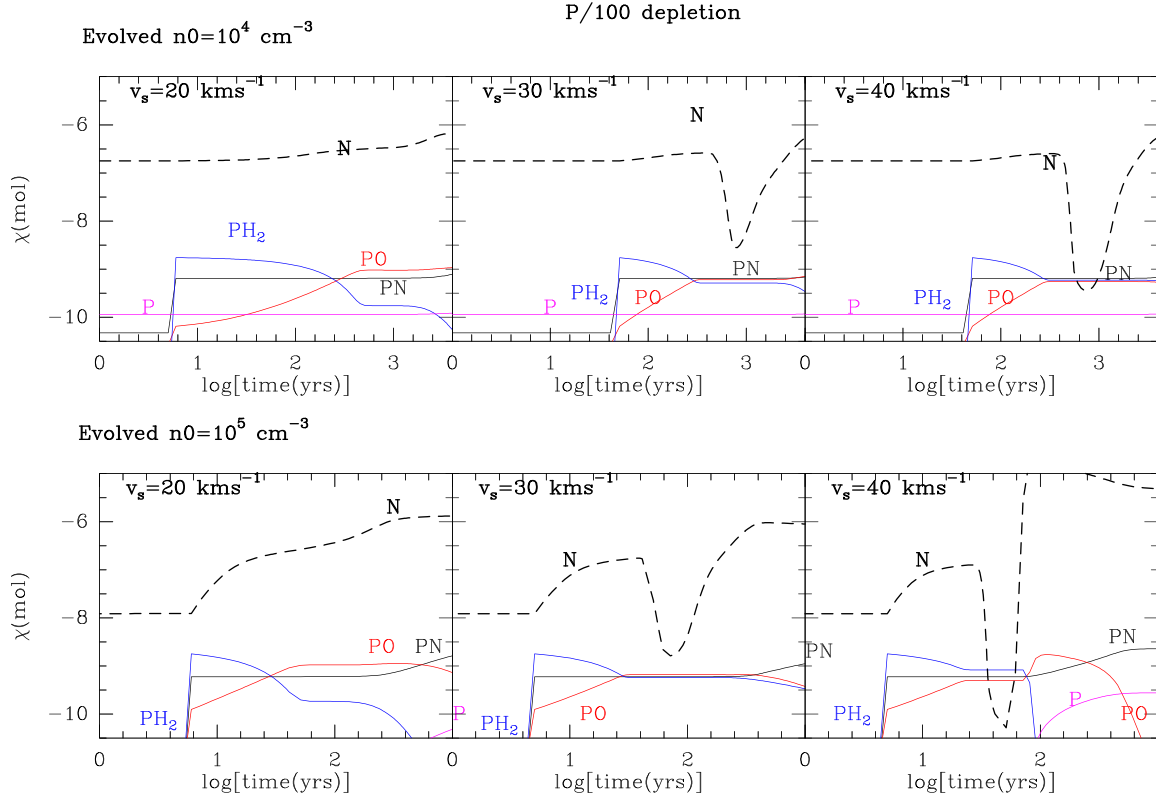[5] http://kida.obs.u-bordeaux1.fr/

Figure 3. Fractional abundances of selected species as a function of time for the shocked phase. In all models, the initial elemental abundance of phosphorous is depleted by a factor of 100 with respect to its solar abundance. The pre-shock phase is long-lived.
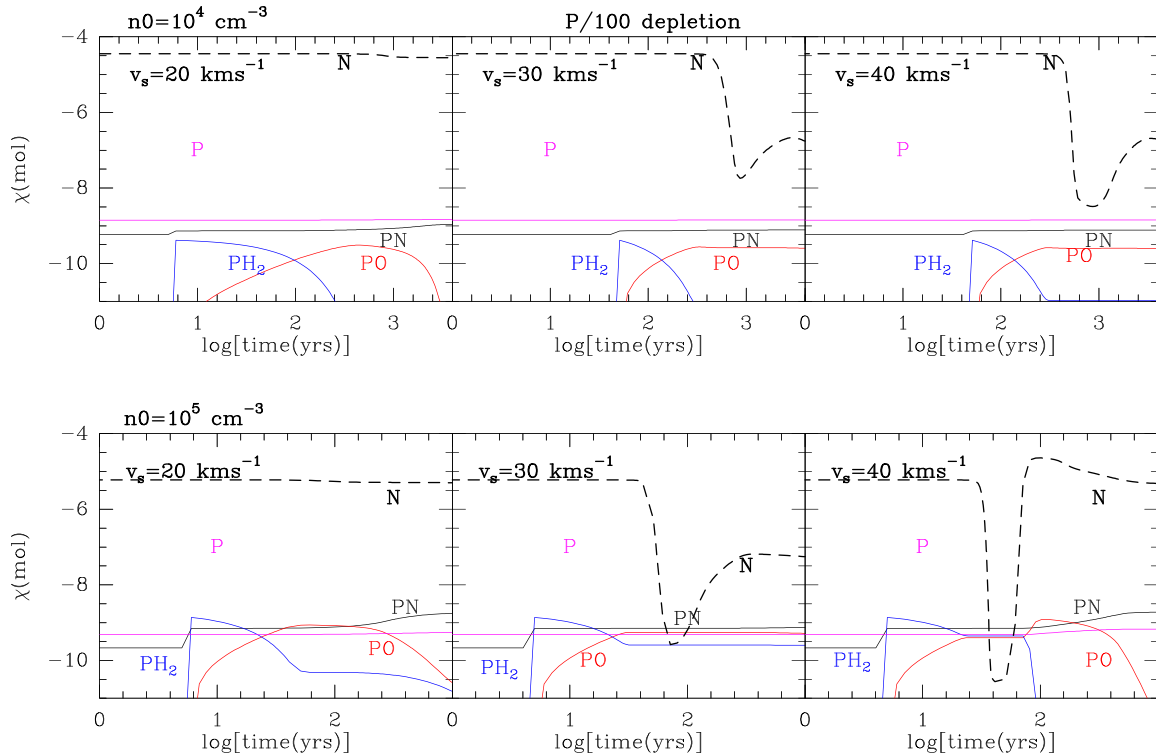

Figure 4. Fractional abundances of selected species as a function of time for the shocked phase. In all models, the initial elemental abundance of phosphorous is depleted by a factor of 100 with respect to its solar abundance. The pre-shock phase is short-lived.

respectively. We note that the magnitude of the depletion effect affects only the overall abundance of P-bearing species.

Our first result is that none of the models where phosphorous is solar can fit the observations, as all phosphorous bearing species are about two orders of magnitude higher than what is observed. Models where the total gas-phase phosphorous is $\sim 10^{-9}$ are therefore favoured.

As can be seen in Fig. 3, we find that PH_2 is immediately released in the gas phase, as a result of the grain mantle sputtering at the passage of shock. PN follows closely the evolution of PH_2, while PO forms gradually and its abundance rises slowly in the shock. This is in agreement with our observations, where there is a clear shift towards more blueshifted velocities for PO than for PN, which is consistent with a delay in the formation of PO in the gas phase with respect to PN.

If the pre-shock phase (Phase I) is short-lived (Fig. 4), we never reach a situation where PO is clearly larger than PN throughout the shock evolution. As explained below, this is due to the lack of significant depletion of atomic N for time-scales <1 Myr. Atomic phosphorus also remains abundant in the gas phase, at abundances of about 10^{-9}, comparable to or larger than that of PN, depending on the pre-shock density. If the pre-shock phase (Phase I) is short-lived, we never reach a situation where PO is clearly larger than PN throughout the shock evolution. This is the reason why Aota & Aikawa (2012) opted for a short-lived pre-shock phase to explain the upper limits of PO measured towards L1157-B1 by Yamaguchi et al. (2011). Given the uncertainties in the derivation of PO and PN abundances, we cannot discard a situation where the PO/PN ratio is simply ≈ 1, however.

A chemical analysis on the formation and destruction of PO and PN shows that the key player in their chemistry is atomic nitrogen (as also found by Aota & Aikawa 2012), which in turn is mainly released from ammonia NH_3 in the shock: for example, for the higher pre-shock densities (10^5 cm^{-3}) and weak shocks (20 km s^{-1}), a significant fraction of atomic nitrogen is still present in the gas phase and hence PO is destroyed by the reaction

$$N + PO \rightarrow PN.$$
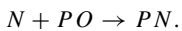
This reaction contributes to ~ 85 per cent to the total destruction of PO. When the shock velocity is higher, about 30 km s^{-1}, the temperature of the neutral fluid is also higher and favours the conversion of N into NH_3, and therefore PO survives in the gas phase for longer. However, at higher velocities (40 km s^{-1}), as also shown in Viti et al. (2011), NH_3 is efficiently destroyed in the post-shock gas, liberating N into the gas phase and augmenting the destruction of PO via N (a route that here contributes to 100 per cent of the PO destruction). This leads to a faster drop for PO. This process requires that the maximum temperature in the shock is larger than 4000 K.

Because the amount of available nitrogen is key to the survival of PO, a higher pre-shock density favours it: for higher densities, more nitrogen is locked on to grains in the form of NH_3. The atomic Nitrogen abundance decreases by ≈ 10 when the pre-shock density increases from 10^4 to 10^5 cm^{-3} (see e.g. Figs 3 and 4). Since from previous discussion in Section 3.2, the terminal velocity of PO is smaller (about -10 km s^{-1}) than the PN one (almost -20 km s^{-1}), the model with a shock velocity of 40 km s^{-1} (bottom right of Fig. 3) is the best match, as PO is destroyed at the end of the post-shock region as a consequence of the destruction of NH_3.

The best-matching models are, in fact, those where the pre-shock phase is longer lived (Fig. 3), again, because atomic nitrogen has more time to get locked in the icy mantles before the arrival of the shock. In all the models from Fig. 3, PN and PO are comparable for most of the dissipation length. The only model for which we find a sharp decrease in abundance in the post-shock region is the model with pre-shock density of 10^5 cm^{-3} and a shock velocity of 40 km s^{-1}. Such a drop occurs at a time of ~ 600 yr and translates into lower terminal velocities of the PO line emission. Models with a shock velocity of 20 and 30 km s^{-1} also indicate a PO abundance drop from the gas phase. This abundance drop occurs at a longer time, however, once passed the dissipation length, which makes it difficult to quantify accurately based on our simple modelling. Because of this, and because similar shock velocities are also required to explain the different line profiles observed towards L1157-B1 for NH_3 and H_2O (Viti et al. 2011), we favour the scenario in which PN and PO are formed in a shock with a velocity of 40 km s^{-1}. Finally, we note that a high pre-shock density also favours the idea that dense clumps along outflows pre-exist the outflow event itself and are not, in fact, formed by compression due to the arrival of the shock (Viti et al. 2004a).

5.3 Comparison with previous results

Using the detection of the PN J = 2–1 line and the non-detection of PO by Yamaguchi et al. (2011) in L1157-B1, Aota & Aikawa (2012) modelled the phosphorous chemistry in the shocked region of L1157-B1 by using a chemical model coupled with the parametric shock model by Jimenez-Serra et al. (2008). These authors searched for shock solutions whereby PN was abundant while PO was not. The wider and richer spectral content of the ASAI data brings more robust constraints on the properties of P-bearing species PO, PN (and PH_3) in L1157-B1, affecting some of their conclusions on the shock properties: their study favours a shock velocity of 20 km s^{-1}, while our results suggest that PN and PO are formed in a 40 km s^{-1} shock. In our model, a maximum temperature of 4000 K is indeed required in the shock to liberate atomic N into the gas phase from NH3 and to destroy PO at higher velocities in the shock (as suggested by the observed different terminal velocities of PN and PO; Section 3.2). Our conclusions on the depletion of elemental phosphorus by a factor of 100 in molecular dark clouds, and of the importance of atomic N in the chemistry of PO and PN, agree with those of Aota & Aikawa (2012).

Recent studies of PN and PO towards the high-mass star-forming regions W51 e1/e2 and W3(OH) by Fontani et al. (2016) and Rivilla et al. (2016) reach conclusions similar to ours: phosphorus appears to be depleted in quiescent molecular gas by more than one order of magnitude. The abundances they derive towards these massive sources are of the order of 10^{-10}, typically one order of magnitude less than towards the shock L1157-B1. Interestingly, they report similar PO/PN abundance ratios ($\simeq 2$–3). Observations with the NOrthern Extended Millimeter Array (NOEMA) array would permit more accurate determination of the depletion factor by resolving the size of the emitting region of PO and PN at a few arcsec scale. Mapping the relative spatial distribution of PO and PN as a function of velocity would permit confirmation of our conclusions on the shock parameters.

6 CONCLUSIONS

We report on a systematic search for P-bearing species towards the solar-type star-forming region L1157. We have unambiguously detected emission from PN and, for the first time, from the pre-biotic

molecule PO in the outflow shock region L1157-B1. No emission from P-bearing species was detected towards the envelope of the protostar L1157-mm. Spectral line profile analysis suggests that the emission originates from the same region as SiO, with a typical size of 15–20 arcsec. The abundances of PO and PN are found comparable, with values of 2.5 and 0.9×10^{-9}, respectively.

A simple modelling using the C-shock code of Jimenez-Serra et al. (2008) coupled the chemical gas–grain model UCL_CHEM (Viti et al. 2004a) allows us to reproduce the main features of PO and PN emission in the shock. Our main conclusions are as follows.

(i) Phosphorus is depleted by about a factor of 100 in the gas phase.

(ii) Atomic Nitrogen plays a key role in the formation and destruction routes of PO and PN

(iii) The observed PO/PN abundance ratio is ≈3, and brings constraints on the duration of the pre-shock phase, which has to be larger than $\simeq 10^6$ yr and the pre-shock density, of the order of 10^5 cm^{-3}.

(iv) The maximum temperature in the shock has to be ∼4000 K in order to account for the difference of terminal velocities between PO and PN.

Follow-up observations at arcsec scale with the NOEMA array would permit probing the model we propose for the formation of PO and PN in the shock. By resolving the size of the emitting region of PO and PN, it would possible to confirm that both species form in different regions of the shock, and to estimate more accurately the phosphorus depletion factor in the gas phase.

ACKNOWLEDGEMENTS

REFERENCES

Agundez M., Cernicharo J., Guélin M., 2007, ApJ, 662, L91
Altwegg K. et al., 2016, Sci. Adv., 2, e1600285
Aota T., Aikawa Y., 2012, ApJ, 761, 74
Asplund M., Grevesse N., Sauval J., Scott P., 2009, ARA&A, 47, 481
Bailleux S., Bogey M., Demuynck C., Liu Y., Walters A., 2002, J. Mol. Spectrosc., 216, 465
Benedettini M. et al., 2013, MNRAS, 436, 179
Cazzoli G., Cludi L., Puzzarini C., 2006, J. Mol. Struct., 780, 260
Codella C. et al., 2010, A&A, 518, L112
De Beck E., Kamiński T., Patel N. A., Young K. H., Gottlieb C. A., Menten K. M., Decin L., 2013, A&A, 558, 132
Draine B. T., Roberge W. G., Dalgarno A., 1983, ApJ, 264, 485
Fontani F., Rivilla V. M., Caselli P., Vasyunin A., Palau A., 2016, ApJ, 822, L30
Gómez-Ruiz A. et al., 2015, MNRAS, 446, 3346
Gueth F., Guilloteau S., Bachiller R., 1998, A&A, 333, 287
Holdship J. et al., 2016, MNRAS, in press
Jenkins E. B., Savage B. D., Spitzer L., 1986, ApJ, 301, 355
Jimenez-Serra I., Caselli P., Martin-Pintado J., Hartquist T. W., 2008, A&A, 482, 549
Kawaguchi K., Saito S., Hirota E., 1983, J. Chem. Phys., 79, 629
Lefloch B. et al., 2012, ApJ, 757, L25
Macía E., 2005, Chem. Soc. Rev., 34, 691
Matthews H. E., Feldman P. A., Bernath P. F., 1987, ApJ, 312, 358
Müller H. S. P., Wood D. E., 2013, J. Phys. Chem. A, 117, 13868
Rawlings J. M. C., Hartquist T. W., Menten K. M., Williams D. A., 1992, MNRAS, 225, 471
Rivilla V. M., Fontani F., Beltran M. T., Vasyunin A., Caselli P., Martíín-Pintado J., Cesaroni R., 2016, ApJ, 826, 161
Tenenbaum E. D., Woolf N. J., Ziurys L. M., 2007, 666, L29
Thorne L. R., Anicich V. G., Prasad S. S., Huntress W. T., Jr., 1984, ApJ, 280, 139
Tobola R., Klos J., Lique F., Chałasiński G., Alexander M. H., 2007, A&A, 468, 1123
Turner B. E., Bally J., 1987, ApJ, 321, L75
Viti S., Codella C., Benedettini M., Bachiller R., 2004a, MNRAS, 350, 1029
Viti S., Collings M. P., Dever J. W., 2004b, MNRAS, 354, 1141
Viti S., Jimenez-Serra I., Yates J. A., Codella C., Vasta M., Caselli P., Lefloch B., Ceccarelli C., 2011, ApJ, 740, L3
Yamaguchi T. et al., 2011, PASJ, 63, L37
Ziurys L., 1987, ApJ, 321, L81

This paper has been typeset from a TEX/LATEX file prepared by the author.